A constrained analysis of the 40Ca(18O,18F)40K direct charge exchange reaction mechanism at 275 Mev

23 April 2024

frontiers in Astronomy and Space Sciences

ORIGINAL RESEARCH
published: 07 May 2021
doi: 10.3389/fspas.2021.659815

A Constrained Analysis of the $^{40}Ca(^{18}O,^{18}F)^{40}K$ Direct Charge Exchange Reaction Mechanism at 275 MeV

Manuela Cavallaro[1], Jessica I. Bellone[1], Salvatore Calabrese[1], Clementina Agodi[1], Stefano Burrello[2], Francesco Cappuzzello[1,3], Diana Carbone[1], Maria Colonna[1], N. Deshmukh[4], H. Lenske[5], A. Spatafora[1,3], L. Acosta[6], P. Amador-Valenzuela[7], T. Borello-Lewin[8], G. A. Brischetto[1,3], D. Calvo[9], V. Capirossi[9,10], E. Chávez[6], I. Ciraldo[1,3], M. Cutuli[1,3], F. Delaunay[11], H. Djapo[12], C. Eke[13], P. Finocchiaro[1], S. Firat[14], M. Fisichella[1], A. Foti[15], M. A. Guazzelli[16], A. Hacisalihoglu[17], F. Iazzi[9,10], L. La Fauci[1,3], R. Linares[18], J. Lubian[18], N. H. Medina[8], M. Moralles[19], J. R. B. Oliveira[8], A. Pakou[20], Luciano Pandola[1], H. Petrascu[21], F. Pinna[9,10], G. Russo[15], O. Sgouros[1], S. O. Solakci[14], V. Soukeras[1], G. Souliotis[22], D. Torresi[1], Salvatore Tudisco[1], A. Yildirin[14] and V. A. B. Zagatto[18] for the NUMEN collaboration*

[1] Istituto Nazionale di Fisica Nucleare, Laboratori Nazionali del Sud, Catania, Italy, [2] Université Paris-Saclay, CNRS/IN2P3, IJCLab, Orsay, France, [3] Dipartimento di Fisica e Astronomia "Ettore Majorana," Università di Catania, Catania, Italy, [4] School of Sciences, Auro University, Surat, India, [5] Department of Physics, University of Giessen, Giessen, Germany, [6] Instituto de Física, Universidad Nacional Autónoma de México, Mexico City, Mexico, [7] Departamento de Aceleradores y Estudio de Materiales, Instituto Nacional de Investigaciones Nucleares—Ocoyoacac, Mexico City, Mexico, [8] Instituto de Fisica, Universidade de São Paulo, São Paulo, Brazil, [9] Istituto Nazionale di Fisica Nucleare, Sezione di Torino, Turin, Italy, [10] Dipartimento Scienza Applicata e Tecnologia, Politecnico di Torino, Turin, Italy, [11] LPC Caen, Normandie Université, ENSICAEN, UNICAEN, CNRS/IN2P3, Caen, France, [12] Institute of Accelerator Technologies, Ankara University, Ankara, Turkey, [13] Department of Mathematics and Science Education, Akdeniz University, Antalya, Turkey, [14] Department of Physics, Akdeniz University, Antalya, Turkey, [15] Istituto Nazionale di Fisica Nucleare, Sezione di Catania, Catania, Italy, [16] Centro Universitario FEI, São Bernardo do Campo, Brazil, [17] Institute of Natural Science, Karadeniz Teknik Universitesi, Trabzon, Turkey, [18] Instituto de Fisica, Universidade Federal Fluminense, Niterói, Brazil, [19] Instituto de Pesquisas Energeticas e Nucleares IPEN/CNEN, São Paulo, Brazil, [20] Department of Physics, University of Ioannina and Hellenic Institute of Nuclear Physics, Ioannina, Greece, [21] IFIN-HH, Bucharest, Romania, [22] Department of Chemistry, University of Athens and Hellenic Institute of Nuclear Physics, Athens, Greece

The $^{40}Ca(^{18}O,^{18}F)^{40}K$ single charge exchange (SCE) reaction is explored at an incident energy of 275 MeV and analyzed consistently by collecting the elastic scattering and inelastic scattering data under the same experimental conditions. Full quantum-mechanical SCE calculations of the direct mechanism are performed by including microscopic nuclear structure inputs and adopting either a bare optical potential or a coupled channel equivalent polarization potential (CCEP) constrained by the elastic and inelastic data. The direct SCE mechanism describes the magnitude and shape of the angular distributions rather well, thus suggesting the suppression of sequential multi-nucleon transfer processes.

Keywords: nuclear physics, charge exchange reactions, elastic scattering, magnetic spectrometer, neutrinoless double beta (0νββ) decay

OPEN ACCESS

Edited by:
Nunzio Itaco, University of Campania Luigi Vanvitelli, Italy

Reviewed by:
Mengoni Daniele, National Institute of Nuclear Physics of Padova, Italy
Pierre Descouvemont, Université libre de Bruxelles, Belgium

****Correspondence:***
Manuela Cavallaro
manuela.cavallaro@lns.infn.it

Specialty section:
This article was submitted to Nuclear Physics, a section of the journal Frontiers in Astronomy and Space Sciences

Received: *28 January 2021*
Accepted: *30 March 2021*
Published: *07 May 2021*

Citation:
Cavallaro M, Bellone JI, Calabrese S, Agodi C, Burrello S, Cappuzzello F, Carbone D, Colonna M, Deshmukh N, Lenske H, Spatafora A, Acosta L, Amador-Valenzuela P, Borello-Lewin T, Brischetto GA, Calvo D, Capirossi V, Chávez E, Ciraldo I, Cutuli M, Delaunay F, Djapo H, Eke C, Finocchiaro P, Firat S, Fisichella M, Foti A, Guazzelli MA, Hacisalihoglu A, Iazzi F, Fauci LL, Linares R, Lubian J, Medina NH, Moralles M, Oliveira JRB, Pakou A, Pandola L, Petrascu H, Pinna F, Russo G, Sgouros O, Solakci SO, Soukeras V, Souliotis G, Torresi D, Tudisco S, Yildirin A and Zagatto VAB (2021) A Constrained Analysis of the $^{40}Ca(^{18}O,^{18}F)^{40}K$ Direct Charge Exchange Reaction Mechanism at 275 MeV. Front. Astron. Space Sci. 8:659815. doi: 10.3389/fspas.2021.659815

INTRODUCTION

Single charge exchange (SCE) reactions are considered to be the best probe to explore the isospin and spin–isospin nuclear response to the strong interaction. Light-ion-induced SCE reactions have been widely investigated (Taddeucci et al., 1987; Osterfeld, 1992; Alford and Spicer, 1998) especially thanks to the high energy resolution (30 keV) achieved in (^{3}He,t) experiments (Fujita et al., 1997, 2007; Douma et al., 2020) which have allowed to study the details of the populated energy spectra, including their relationships with beta decay transition strengths (Fujita et al., 2011; Frekers et al., 2013; Diel et al., 2019). The use of light-ion-induced SCE reactions for the spectroscopic studies of Fermi ($J^\pi = 0^+$; $L = 0$, $T = 1$, $S = 0$) and Gamow–Teller ($J^\pi = 1^+$; $L = 0$, $T = 1$, $S = 1$) excitations is well-established. Recent studies have also shown a sensitivity of (^{3}He,t) reactions to higher multipoles, such as the spin dipole ($J^\pi = 2^-$; $L = 1$, $T = 1$, $S = 1$) (Ejiri et al., 2014; Akimune et al., 2020). The isospin response at high multipolarity has attracted interest in the last few years in view of its possible connection to neutrinoless double beta decay ($0\nu\beta\beta$) nuclear matrix elements (NMEs), where indeed higher multipoles are expected to play a relevant role in an intermediate virtual state (Ejiri et al., 2019). Ordinary muon capture (OMC) techniques, despite the moderate energy resolution of the order of few MeV, have been recently developed to explore nuclear high multipoles stimulated by isospin weak interaction operators (Ejiri, 2005; Jokiniemi et al., 2019).

In this perspective, heavy-ion-induced SCE reactions are particularly interesting because of their enhanced probability to populate high-spin states, due to the large momentum transferred from the heavy projectile to the target even at forward scattering angles. Hence, heavy-ion SCE reactions are expected to provide a relevant contribution to our understanding of the matrix elements of nuclear multipole transitions (Lenske et al., 2018, 2019). In this case, the achievable energy resolution is a few hundred keV, mainly limited by energy straggling due to the projectile–target interaction, which is often enough to allow the separation of low-lying states in the inclusive spectra. Different heavy-ion probes have been proposed in the years, mainly induced by ^{6,7}Li, ^{12,13}C, ^{48}Ti beams at energies above the Coulomb barrier (Lenske et al., 2019). The main findings concern the competition between direct meson exchange and sequential nucleonic transfer mechanisms depending on the specific dynamical conditions. When the direct mechanism is dominant, a proportionality of SCE cross sections with beta decay strengths is found and a general trend to favor the population of unnatural parity transitions is observed (Cappuzzello et al., 2004a). Not much is known about the (^{18}O,^{18}F) SCE reaction, which is discussed in the present paper. Such a probe has been studied on the ^{28}Si and ^{36}S targets from 3 to 19.6 A MeV (Kim et al., 1979; Horen et al., 1986; Fifield et al., 1993). In all cases, a significant role of the direct mechanism has been deduced, especially at the highest beam energies, but uncertainties in the adopted models for the nuclear structure and reaction inputs did not allow to draw any firm conclusion.

The study of such SCE reactions is of crucial importance in the NUMEN and NURE projects (Cappuzzello et al., 2015a, 2018; Cavallaro et al., 2017) at the INFN-LNS laboratory, which aims at investigating double-charge exchange (DCE) reactions (^{18}O,^{18}Ne) and (^{20}Ne,^{20}O) to an unprecedented level of accuracy, both from the experiment and theory side, in view of their connections with $0\nu\beta\beta$ decay. The key aspects of this research program are the similarities between the two classes of processes, DCE and $0\nu\beta\beta$, both characterized by the exchange of two units of isospin between the initial state and the final state, although mediated by the strong interaction and the weak interaction, respectively (Cappuzzello and Cavallaro, 2020).

A theory for heavy-ion SCE and DCE reactions, describing the two kinds of reaction in a unified manner, was missing up to few years ago and is presently under development within the NUMEN activities (Lenske et al., 2018, 2019; Santopinto et al., 2018; Bellone et al., 2020; Carbone et al., 2020; Ferreira et al., 2021; Burrello et al., in preparation). The competition between the direct mechanisms, mediated by the exchange of one (SCE) or two (DCE) charged mesons between the projectile and target and probing the isospin structure of the ions, and the sequential transfer of protons and neutrons, probing the mean field structure of the involved nuclei, is one of the topics of this research. In particular, Bellone et al. (2020) demonstrated that the (^{18}O,^{18}F) cross section is fundamental to constrain the DCE sequential meson exchange mechanism along the ^{18}O $\rightarrow$ ^{18}F $\rightarrow$ ^{18}Ne transition. Moreover, the experimental measurement and analysis of the elastic scattering and inelastic scattering cross sections for the same projectile–target system is crucial to constrain the SCE and DCE calculations. Indeed, the projectile–target nucleus-nucleus potential needs to be accurately modeled both in the entrance [initial state interaction (ISI)] and exit [final state interaction (FSI)] channels (Spatafora et al., 2019; Carbone et al., 2021; La Fauci et al., submitted).

A case of interest for a description of charge exchange cross sections is the ^{40}Ca(^{18}O,^{18}F)^{40}K reaction at an incident energy of 275 MeV for which the theoretical formalism and the details of a microscopic quantum-mechanical calculation were reported by Lenske et al. (2018). Such an approach includes a nuclear structure part modeled by quasi-particle random phase approximation- (QRPA-) based transition densities, and a reaction part via distorted wave Born approximation (DWBA) cross section calculations. Here, we provide for the first time the experimental cross section angular distribution data and discuss their comparison with the theoretical calculations. Contextually, the elastic and inelastic scattering of ^{18}O beam on ^{40}Ca target at the same bombarding energy were measured in a wide momentum transfer range and studied to extract the optical potential to be used in the SCE calculations. The importance of experimental constraints coming from the elastic scattering data to the determination of the ion–ion interaction was already stressed by Lenske et al. (2018). However, such information was missing in that work and is available here for the first time. The effect of the couplings with inelastic excitations is also explored here.

EXPERIMENT AND DATA REDUCTION

The $^{40}Ca(^{18}O,^{18}F)^{40}K$ charge exchange reaction was measured at INFN-Laboratori Nazionali del Sud in Catania (Italy). A beam of $^{18}O^{4+}$ ions, extracted by the K800 Superconducting Cyclotron accelerator, bombarded a 280 ± 14 μg/cm^2 natural calcium (96.9% ^{40}Ca) target at an incident energy of 275 MeV. The calcium material for the target was evaporated on a carbon backing of 25 μg/cm^2 thick, and a further carbon layer of 15 μg/cm^2 was evaporated on the top of the calcium layer to reduce oxidation processes. The $^{18}O + ^{40}Ca$ elastic scattering and inelastic scattering were measured in a dedicated run using a 250 ± 12 μg/cm^2 thick calcium target evaporated on 47 μg/cm^2 carbon backing. A Faraday cup located inside a scattering chamber and 15 cm downstream of the target was used to collect the beam charge. An electron suppressor polarized at −200 V and a low-noise charge integrator allowed a charge collection accuracy better than 10%. The ejectiles produced in the collisions were selected by the MAGNEX large acceptance spectrometer (Cappuzzello et al., 2016) and identified by its focal plane detector (Cavallaro et al., 2012; Torresi et al., 2021). For the charge exchange measurement, the optical axis of the spectrometer was located at $\theta_{opt} = +7°$ with respect to the beam direction. Thanks to the MAGNEX angular acceptance, an angular range of $3° < \theta_{lab} < 9°$ in the laboratory reference frame was explored in a single angular setting. For the measurement of elastic scattering and inelastic scattering, the optical axis of MAGNEX was set at $\theta_{opt} = +8°$, $+14°$, and $+18°$ in three different acquisition runs, exploring an overall angular range of $3° < \theta_{lab} < 19°$. The procedure to reduce the collected data and extract the energy spectra and the cross section angular distributions for the measured transitions is described in detail by Cappuzzello et al. (2010), Cappuzzello et al. (2011), Cappuzzello et al. (2014), Calabrese et al. (2020), Cavallaro et al. (2011), and Carbone (2015).

In **Figure 1**, an example of a measured spectrum is shown as a function of excitation energy $E_x = Q_0 - Q$ (where Q is the reaction Q-value, $Q_0 = 0$ for elastic scattering) for the $^{18}O+^{40}Ca$ scattering in the angular region $8.2° < \theta_{lab} < 9.0°$. The peaks related to the transition to the 0^+ ^{40}Ca ground state and to

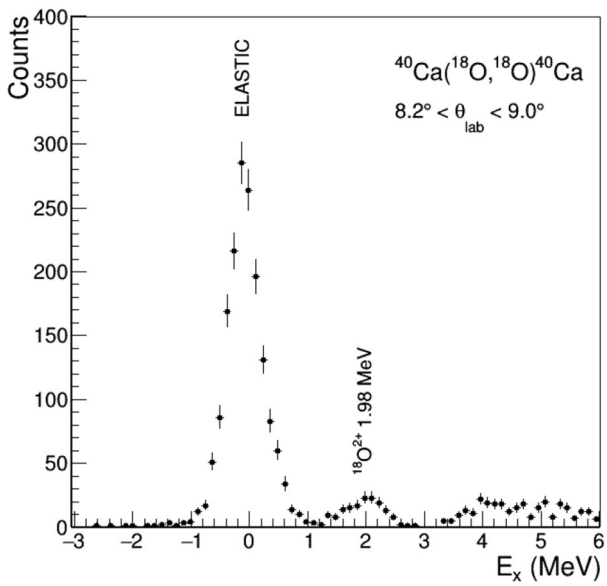

FIGURE 1 | Excitation energy spectrum of ^{40}Ca obtained in the $^{18}O + ^{40}Ca$ elastic scattering and inelastic scattering at an incident energy of 275 MeV and $8.2° < \theta_{lab} < 9.0°$.

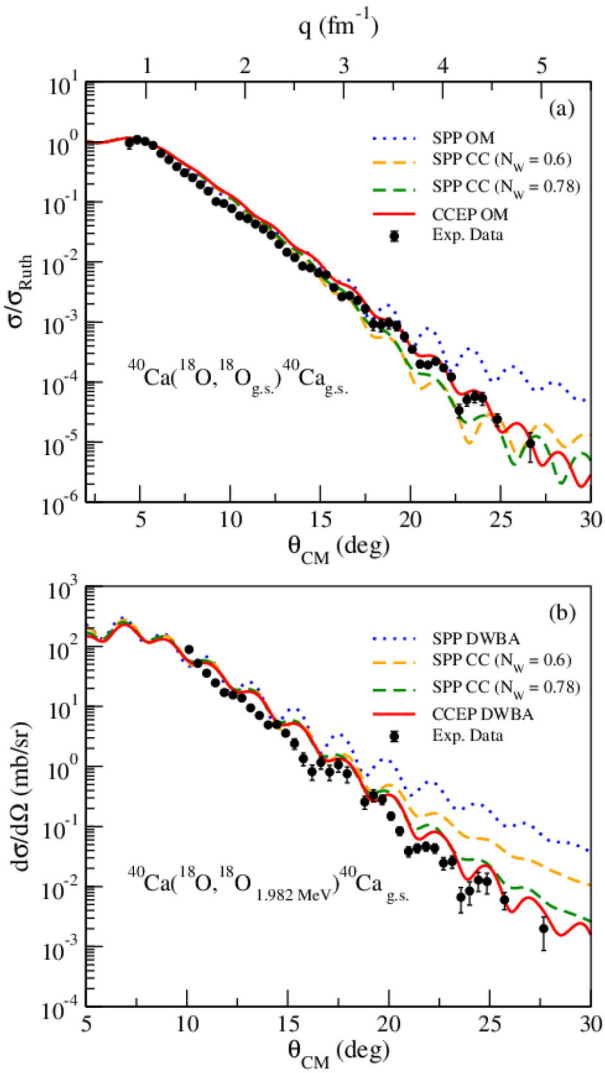

FIGURE 2 | (A) Cross section angular distribution of the $^{18}O + ^{40}Ca$ elastic scattering at 275 MeV in terms of its ratio to the Rutherford cross section σ_{Ruth}. **(B)** Angular distribution of the inelastic channel $^{40}Ca(^{18}O,^{18}O_{1.982})^{40}Ca_{g.s.}$ In both plots, the blue dotted line shows the optical model (OM; for elastic) and distorted wave Born approximation (DWBA; for inelastic) calculations with São Paulo potential (SPP), the orange dashed line shows the coupled channel (CC) calculations with SPP and $N_W = 0.6$, the green dashed line shows the CC calculations with SPP and $N_W = 0.78$, and the red solid line shows the OM and DWBA calculations with coupled channel equivalent polarization potential (CCEP).

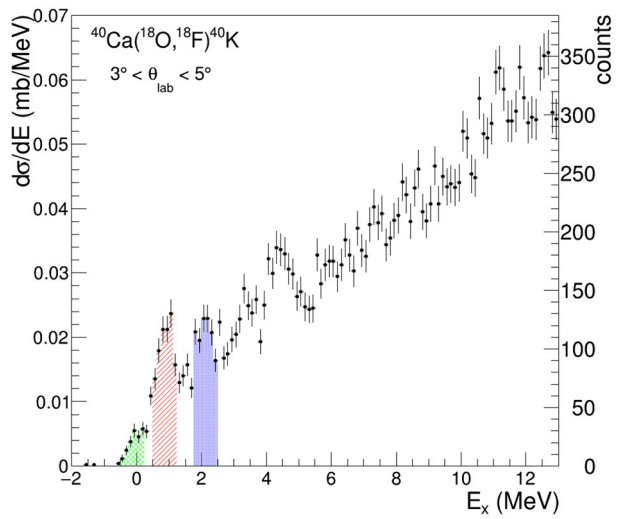

FIGURE 3 | Excitation energy spectrum of the ^{40}Ca(^{18}O, ^{18}F)^{40}K charge exchange reaction at 275 MeV and $3^\circ < \theta_{lab} < 5^\circ$. The three hatched areas indicate the regions of interest for the study of the angular distributions.

the first 2^+ ^{18}O excited state at $E_x = 1.982$ MeV are clearly visible. The structures above $E_x = 3$ MeV are due to unresolved excitations of both ejectile and residual nuclei. The contributions arising due to the carbon and oxygen impurities in the target are expected at $E_x > 6$ and $E_x > 4$ MeV, respectively, so not present in the range of the explored transitions. An energy resolution of about 500 keV (full width at half maximum) is measured.

The cross section angular distribution for the ^{18}O + ^{40}Ca elastic scattering, expressed in terms of its ratio to the Rutherford cross section, is shown in **Figure 2A**. The corresponding scale of transferred linear momentum q is also given. The angular distribution for the inelastic scattering to the first excited state of ^{18}O at 1.982 MeV is shown in **Figure 2B**.

The ^{40}K excitation energy spectrum $E_x = Q_0 - Q$ (where Q is the reaction Q-value and Q_0 the ground state to ground state Q-value) extracted from the ^{40}Ca(^{18}O,^{18}F)^{40}K SCE measurement in the angular region of $3^\circ < \theta_{lab} < 5^\circ$ is shown in **Figure 3**. Both counts and energy differential cross section $d\sigma/dE$ in the absolute value (mb/MeV) are indicated in two scales. Some structures are observed in the low excitation energy region; however, the limited resolution and the high-level density do not allow to isolate single transitions. The groups of levels belonging to the three energy regions indicated in **Figure 3** as well as the corresponding integrated cross sections in the angular interval of $4.8^\circ < \theta_{CM} < 11.3^\circ$ are listed in **Table 1**.

The angular distributions for the SCE cross section extracted in the three regions of interest of the ^{18}F+^{40}K excitation energy sketched in **Figure 3** are shown in **Figure 4**. In particular, the ground state region (including the unresolved transitions to the ground state and the first excited state of ^{40}K at 0.029 MeV), the region at energies of 0.5 MeV $< E_x <$ 1.2 MeV and the region at energies of 1.7 MeV $< E_x <$ 2.6 MeV are explored. For the extraction of the cross section in the ground state region, a Gaussian fitting procedure was performed for each angular bin.

The error bars reported in the experimental data in **Figures 2**, **4** include the statistical contribution and the uncertainties coming from the determination of the solid angle intervals. An overall uncertainty of about 10%, due to the determination of charge collection and target thickness, is not shown in **Figures 2**, **4** as it is common to all data points in the angular distributions.

ANALYSIS OF THE ELASTIC AND INELASTIC SCATTERING AND DETERMINATION OF THE OPTICAL POTENTIAL

The measured angular distributions of the elastic and inelastic experimental cross section are compared with the quantum-mechanical optical model (OM), DWBA, and coupled channel (CC) calculations, using the FRESCO code (Thompson, 1988). The double-folding São Paulo potential (V_{SPP}) (Chamon et al., 2002) is adopted as the real part of a complex optical potential $U(r) = V_{SPP}(r) + i\, N_W\, V_{SPP}(r)$. The imaginary part is assumed with the same shape of the real one scaled by a factor $N_W = 0.78$, as typically done, for example, in Alvarez et al. (2003), Spatafora et al. (2019), and Oliveira et al. (2013). For the CC calculations, the results obtained by using a smaller scaling factor, $N_W = 0.6$ (Pereira et al., 2009), are also shown and commented in the following. In the double-folding procedure, two-parameter Fermi distributions are adopted to describe the projectile and target matter densities, with radius and diffuseness obtained from systematic analyses (Chamon et al., 2002). In particular, the diffuseness of the matter density of the projectile is set to $a_p = 0.61$ fm, which is increased by 10% with respect to SPP systematics ($a_p = 0.56$ fm), as commonly done for ^{18}O projectile (Crema et al., 2011; Cavallaro et al., 2013; Cappuzzello et al., 2015b; Ermamatov et al., 2016, 2017; Carbone et al., 2017; Paes et al., 2017; Cardozo et al., 2018; Linares et al., 2018; Fonseca et al., 2019).

The couplings introduced in the DWBA and CC calculations account for the collective low-lying quadrupole and octupole transitions. Namely, we consider the first ^{18}O(2^+) excited state at $E_x = 1.982$ MeV, and the first ^{40}Ca(3^-) and ^{40}Ca(2^+) excited states, at 3.737 MeV and 3.904 MeV, respectively. The adopted coupling scheme is sketched in **Figure 5**.

Both DWBA and CC calculations are performed within a rotational model. Calculations within a vibrational model do not give relevant differences in the results. Reduced transition probabilities B(E2; $0^+ \rightarrow 2^+$) = 0.0043 e^2b^2 for ^{18}O, B(E3 $0^+ \rightarrow 3^-$) = 0.0184 e^2b^3 and B(E2; $0^+ \rightarrow 2^+$) = 0.00924 e^2b^2 for ^{40}Ca are taken from Pritychenko et al. (2016), Pritychenko et al. (2017), and Kibedi and Spear (2002) and used to describe the strength of Coulomb deformation of both the projectile and target (Satchler, 1983; Khoa and Satchler, 2000).

Nuclear deformations (for the multipolarity λ) are described in terms of a first-order derivative of the potential $U(r)$, which is used to describe the corresponding elastic channel:

TABLE 1 | Transitions expected for the three regions of interest of the $^{40}Ca(^{18}O,^{18}F)^{40}K$ energy spectrum as indicated in **Figure 3**.

Excitation energy region (MeV)	Final channel	Calculated cross section (μb)	Sum of calculated cross section (μb)	Experimental cross section (μb)
−0.5 – 0.2	$^{18}F_{g.s.}(1^+) + ^{40}K_{g.s.}(4^-)$	0.51	0.92	5.6 ± 0.6
	$^{18}F_{g.s.}(1^+) + ^{40}K_{0.029}(3^-)$	0.41		
0.5 – 1.2	$^{18}F_{g.s.}(1+) + ^{40}K_{0.800}(2^-)$	8.7	9.6	25 ± 2
	$^{18}F_{g.s.}(1^+) + ^{40}K_{0.891}(5^-)$	$4.7\cdot10^{-2}$		
	$^{18}F_{0.937}(3^+) + ^{40}K_{g.s.}(4^-)$	0.42		
	$^{18}F_{0.937}(3^+) + ^{40}K_{0.029}(3^-)$	$8.9\cdot10^{-2}$		
	$^{18}F_{1.042}(0^+) + ^{40}K_{0.029}(3^-)$	0.19		
	$^{18}F_{1.121}(5^+) + ^{40}K_{g.s.}(4^-)$	$9.6\cdot10^{-2}$		
	$^{18}F_{1.121}(5^+) + ^{40}K_{0.029}(3^-)$	$8.2\cdot10^{-3}$		
1.7 – 2.6	$^{18}F_{g.s.}(1^+) + ^{40}K_{1.959}(2^+)$	$1.3\cdot10^{-2}$	23	31 ± 2
	$^{18}F_{g.s.}(1^+) + ^{40}K_{2.047}(2^-)$	4.2		
	$^{18}F_{g.s.}(1^+) + ^{40}K_{2.070}(3^-)$	0.18		
	$^{18}F_{g.s.}(1^+) + ^{40}K_{2.104}(1^-)$	3.8		
	$^{18}F_{g.s.}(1^+) + ^{40}K_{2.260}(3^+)$	$3.5\cdot10^{-2}$		
	$^{18}F_{g.s.}(1^+) + ^{40}K_{2.290}(1^+)$	0.13		
	$^{18}F_{g.s.}(1^+) + ^{40}K_{2.290}(3^-)$	1.2		
	$^{18}F_{g.s.}(1^+) + ^{40}K_{2.397}(4^-)$	1.8		
	$^{18}F_{g.s.}(1^+) + ^{40}K_{2.419}(2^-)$	6.8		
	$^{18}F_{g.s.}(1^+) + ^{40}K_{2.543}(7^+)$	$4.1\cdot10^{-4}$		
	$^{18}F_{g.s.}(1^+) + ^{40}K_{2.576}(2^+)$	$4.6\cdot10^{-3}$		
	$^{18}F_{g.s.}(1^+) + ^{40}K_{2.626}(0^-)$	1.2		
	$^{18}F_{0.937}(3^+) + ^{40}K_{0.800}(2^-)$	2.1		
	$^{18}F_{0.937}(3^+) + ^{40}K_{0.891}(5^-)$	$4.3\cdot10^{-2}$		
	$^{18}F_{1.041}(0^+) + ^{40}K_{0.891}(5^-)$	0.26		
	$^{18}F_{1.121}(5^+) + ^{40}K_{0.800}(2^-)$	0.17		
	$^{18}F_{1.121}(5^+) + ^{40}K_{0.891}(5^-)$	$1.7\cdot10^{-2}$		
	$^{18}F_{1.701}(1^+) + ^{40}K_{g.s.}(4^-)$	$3.7\cdot10^{-2}$		
	$^{18}F_{1.701}(1^+) + ^{40}K_{0.029}(3^-)$	$2.8\cdot10^{-2}$		
	$^{18}F_{1.701}(1^+) + ^{40}K_{0.800}(2^-)$	1.0		
	$^{18}F_{1.701}(1^+) + ^{40}K_{0.891}(5^-)$	$1.7\cdot10^{-3}$		
	$^{18}F_{2.101}(2^-) + ^{40}K_{g.s.}(4^-)$	$2.4\cdot10^{-4}$		
	$^{18}F_{2.101}(2^-) + ^{40}K_{0.029}(3^-)$	$1.1\cdot10^{-4}$		
	$^{18}F_{2.523}(2^+) + ^{40}K_{g.s.}(4^-)$	$6.8\cdot10^{-5}$		
	$^{18}F_{2.523}(2^+) + ^{40}K_{0.029}(3^-)$	$4.8\cdot10^{-2}$		

The third and fourth columns give the calculated cross sections in the angular region of $4.8^\circ < \theta_{CM} < 11.3^\circ$ for each individual transition and summed over the three energy intervals, respectively. The last column gives the measured cross sections integrated in the same angular interval.

$$V_\lambda(r) = -\frac{\delta_\lambda}{\sqrt{4\pi}}\frac{dU(r)}{dr} \tag{1}$$

The strength of the deformation is embedded in the deformation length δ_λ (Satchler, 1983):

$$\delta_\lambda = \beta_\lambda R_V = \frac{4\pi}{3Ze}\frac{\sqrt{(2I+1)\,B(E\lambda;\, I\to I')}}{R_V^{\lambda-1}} \tag{2}$$

where β_λ is the deformation parameter characterizing the transition (of multipole λ) of the given nucleus of charge Ze and is deduced from the electric reduced transition probability $B(E\lambda;\, I \to I')$ from a state of spin I to a state of spin I', and $R_V = 3.73$ fm is the radius of the real part of the adopted optical potential $U(r)$, extracted from its fit with a Woods–Saxon shape (Satchler, 1983). For the imaginary coupling potentials, the same radial form factors are assumed. Exploratory calculations changing the method for the determination of R_V or introducing a N/Z correction factor in Equation (2) to account for possible differences in the density profiles for neutrons and protons (Satchler, 1983), give very similar results, within the quoted uncertainty of $B(E_\lambda;\, I\to I')$ (Kibedi and Spear, 2002; Pritychenko et al., 2016, 2017).

The results of the calculations are compared with the experimental data in **Figure 2**, where all the theoretical curves are folded with the experimental angular resolution (∼0.9° in the center of mass reference frame). The OM and DWBA calculations including São Paulo-derived optical potential

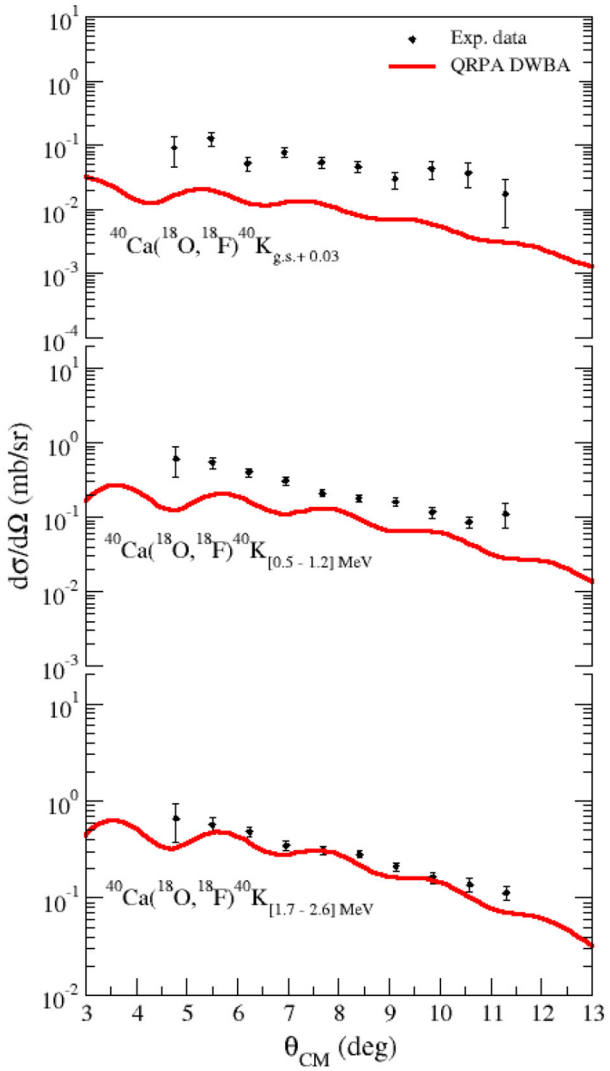

FIGURE 4 | Angular distributions for the $^{40}Ca(^{18}O,^{18}F)^{40}K$ transitions corresponding to the three selected regions in the single charge exchange (SCE) spectrum sketched in **Figure 3**. The red curves are the sum of the cross sections associated to the different transitions belonging to the three regions resulting from the quasi-particle random phase approximation (QRPA) DWBA calculations.

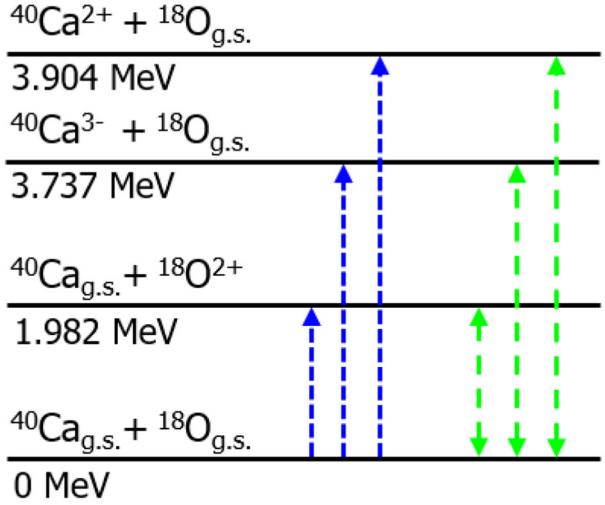

FIGURE 5 | Coupling scheme adopted in the DWBA (blue dotted single arrows) and CC (green dashed double arrows) calculations in the present work. In DWBA, the single arrows sketch that back coupling effects are not included.

describe reasonably well the experimental cross sections at small angles, showing an oscillatory pattern, which is more pronounced than the experimental data and a general overestimation of the data especially at larger angles and momentum transfer ($q >$ 4 fm^{-1}). This behavior resembles the one found in the similar analyses (Zagatto et al., 2018; Spatafora et al., 2019; Carbone et al., 2021; La Fauci et al., submitted; Burrello et al., in preparation) and is due to the lack of important couplings of elastic channel with inelastic channels.

The results of the CC calculations, also reported in **Figure 2**, show that the explored cross sections are affected by the couplings among the selected channels. The main effect is to reduce the cross section, especially at a large momentum transfer. Moreover, the couplings damp the oscillations and slightly shift the positions of the minima toward larger scattering angles, thus improving the description of the data. The coupling to the first 2^+ excited state of the ^{18}O projectile, keeping the target in its ground state, gives a main contribution to the elastic channel. Nonetheless, the explicit inclusion of the coupling to the first 3^- state of ^{40}Ca, keeping the projectile in its ground state, improves the description of the slope of the inelastic cross section (Ohkubo and Hirabayashi, 2014; Cappuzzello et al., 2016; Zagatto et al., 2018). We note that the calculations with N_W = 0.78 better describe the experimental data both in absolute cross section and shape of the angular distributions compared to those obtained assuming N_W = 0.6, which is often used in large-scale CC calculations (Pereira et al., 2009). The larger value for the N_W scaling factor, also reported by Spatafora et al. (2019) and Zagatto et al. (2018), may be explained due to the few states included in the present coupling scheme (see **Figure 5**) and it is compatible with uncertainties in the adopted B(E2) and B(E3) strengths.

As mentioned above, a proper description of the experimental elastic scattering and inelastic scattering data in the fully explored transferred momentum range is achieved, thanks to the introduction of couplings to inelastic channels. This result indicates that also the optical potential necessary for the description of the other quasi-elastic reaction channels induced by the same projectile and target at the same incident energy and angular momentum transfer should account for these couplings. However, it is evident that higher-order effects as introduced by CC calculations are most important for strong channel couplings as, e.g., the coupling of low-lying vibrational or rotational inelastic excitations to the elastic ground state channel. Since the SCE channels are rather weakly coupled to the other configurations, they are well-described already in a first-order DWBA approach. Moreover, in a CC description, the form

TABLE 2 | Volume integrals per interacting pair and root mean square radii for the real (V) part and imaginary (W) part of the São Paulo potential (SPP) and coupled channel equivalent polarization potential (CCEP) optical potentials adopted in the calculations.

	J_v (MeV fm^3)	J_W (MeV fm^3)	$\sqrt{\langle R_V^2 \rangle}$ (fm)	$\sqrt{\langle R_W^2 \rangle}$ (fm)
SPP	−346.1	−269.9	4.75	4.75
CCEP	−233.7	−205.6	4.38	4.59

factors describing each considered reaction channel should come from consistent nuclear structure models. Developments in that direction are the subject of ongoing theory projects and will be discussed elsewhere.

In this view, following the approach of Thompson et al. (1989), we have implicitly incorporated the effect of channel couplings in the elastic optical potential by means of an effective polarization potential term. In general, the formal theory gives a polarization potential, which is not only complex and energy dependent but also non-local and angular momentum dependent. The approach of Thompson et al. (1989), instead, produces an average local and L-independent polarization potential named trivially equivalent local potential (TELP). Adding the TELP to the São Paulo bare optical potential ($V_{\rm SPP}$) used in CC calculations, we get a CCEP (Thompson et al., 1985; Rangel et al., 2016). Such CCEP has been used herein in the OM and DWBA calculations for the elastic scattering and inelastic scattering, respectively, and in the DWBA calculations for the SCE channel described in Section The Charge Exchange Reaction Channel. We emphasize that, in the TELP approach, the effect of couplings is derived from a CC solution of the scattering problem, guaranteeing that the physics of coupling on average is accounted for. Thus, this method is more accurate than the common procedure to scale the imaginary part or slightly modify the geometry of the optical potential (Lubian and Nunes, 2007).

The elastic scattering and inelastic scattering experimental data are compared with the OM and DWBA calculations, respectively, using the CCEP optical potential in **Figure 2**. It is evident that the introduction of the polarization potential is essential to reproduce the experimental cross section even in an OM and a DWBA approach. We stress that in the present work the use of a CCEP has been introduced in view of its application to the SCE and DCE analyses. For the elastic scattering and inelastic scattering studies, it would not be necessary, since CC calculations are feasible and, indeed, have been performed.

The volume integrals and root mean square radii obtained for the SPP and CCEP potentials here adopted are listed in **Table 2**. The results agree with the values known from systematic studies (Satchler, 1983), confirming a very satisfactory description of the optical potential properties.

THE CHARGE EXCHANGE REACTION CHANNEL

As discussed in the introduction, the $^{40}Ca(^{18}O,^{18}F)^{40}K$ SCE reaction could proceed via two mechanisms: one mediated by charged meson exchange (direct SCE) and one governed by mean field interaction among the interacting nucleons (sequential multi-nucleon transfer). In the present work, we show the calculations performed for the former mechanism, which is the one of main interest in view of DCE studies. Calculations are performed within a framework of DWBA, where the cross section in a center of mass rest frame is given by the expression:

$$\frac{d^2\sigma}{dE_x d\Omega} = \frac{E_\alpha E_\beta}{\left(2\pi\hbar^2c^2\right)^2}\frac{k_\beta}{k_\alpha}\frac{1}{(2J_A+1)\,(2J_a+1)} \sum\nolimits_{M_A,\,M_a,M_B,M_b}\left|\int d^3r\,\chi^*_{\beta,\mathbf{k}_\beta}(r)\,F^{(SCE)}_{\alpha\beta}(\mathbf{r})\,\chi_{\alpha,\mathbf{k}_\alpha}(\mathbf{r})\right|^2 \tag{3}$$

where E_α (E_β) and k_α (k_β) denote the energy and relative momentum in the entrance $\alpha = a + A$ (exit $\beta = b + B$) channel; χ_α (χ_β) is the distorted wave, accounting for the initial (final) state interaction, i.e., it is the solution of the Schroedinger equation for the Hamiltonian including Coulomb and optical potential (CCEP in the present study) of the entrance (exit) channel. $F^{(SCE)}_{\alpha\beta}(\mathbf{r})$ is the SCE form factor, given by the folding of the nucleon–nucleon effective local interaction potential $V_{\rm NN}(r)$ and the one-body transition densities of projectile and target nuclei $\rho(r)$.

The effective local nucleon–nucleon direct and exchange interaction potential $V_{\rm NN}(r)$ contains both central and tensor components. It is parameterized by the sum of three Yukawa functions, with parameters coming from a proper interpolation procedure (Lenske, 1988) between two different parameterizations: (i) the G-matrix calculated by solving the Bethe–Salpeter equation with Paris nucleon–nucleon potential for E/A $\leq$ 10 MeV (Anantaraman et al., 1983) and (ii) the Franey–Love parameterization of effective nucleon–nucleon T-matrix for E/A $\geq$ 50 MeV (Franey and Love, 1985). The one-body transition densities $\rho(r)$ are the matrix elements of the one-body operator describing SCE transitions in the projectile and target nuclei (Lenske et al., 2018). These transition densities are calculated within an extended QRPA framework, going beyond the standard approach by accounting for the coupling of the two-quasi-particle configurations to core excitations by polarization self-energies. Residual interactions are determined self-consistently in the context of Fermi-liquid theory. The single quasi-particle states are derived from Hartree–Fock–Bogoliubov (HFB) calculations with state-dependent pairing gaps, describing the ground state properties of the involved nuclei very accurately (Lenske and Tsoneva, 2019). The HFB wave functions and the QRPA configuration amplitudes are used to construct the radial transitions densities, entering finally into the charge exchange transition form factors.

Calculations are performed in terms of the partial wave decomposition of distorted waves and the multipole expansion of the form factor, which is a quite standard procedure (Satchler, 1983). Detailed information on the adopted theoretical modeling is given by Lenske et al. (2018). This approach has been successfully used to also study other heavy-ion-induced SCE

reactions (Cappuzzello et al., 2004a,b; Nociforo et al., 2006; Cavallaro, 2011).

On the reaction side, we performed the DWBA calculations using the CCEP optical potential defined in Section 3 for the three excitation energy ranges for which experimental angular distributions have been extracted. The cross sections corresponding to transitions to different excited states are calculated by using the HIDEX code (Lenske, private communication). The calculations shown in **Figure 4** represent the sum of the angular distributions of the SCE reactions leading to all the possible excited states experimentally populated both by the ejectile and residual nucleus with total excitation energy within the above-mentioned three ranges. These exit channels are listed in **Table 1**, together with the corresponding values of the calculated cross section integrated in the same angular range explored by the data.

Table 1 shows that in the first region of interest, the transitions to the 4^- ground state and 3^- excited state of ^{40}K at 0.029 MeV, with the ^{18}F ejectile at its 1^+ ground state, give comparable contributions. In the [0.5, 1.7] MeV region, the transition to the first 2^- state of ^{40}K at 0.800 MeV and to $^{18}F_{g.s.}(1^+)$ dominates over the other transitions. Conversely, in the [1.7, 2.6] MeV energy range, several multipolarities are comparable in magnitude, even if the cross sections of the transitions to the 2^- states of ^{40}K at 2.047 and 2.419 MeV, with ejectile $^{18}F_{g.s.}(1^+)$, are somewhat larger than the others.

An interesting result comes out from a comparison of the calculated cross sections for the 2^-,3^-,4^-, and 5^- multiplet of states at 0.800, 0.029, 0.0, and 0.891 MeV, respectively. Although these states refer to the same particle-hole structure with one neutron in the $1f_{7/2}$ orbital coupled to a $1d_{3/2}$ proton hole, the calculated cross sections strongly enhance the 2^-. Indeed, the 2^- cross section is larger than the 3^-, 4^-, and 5^-, by a factor of 21, 17, and 185, respectively. A close inspection of the calculated form factors reveals that the $(L = 1, S = 1)$-component of the 2^- transition carries a certain amount of collectivity, reminiscent of the spin-dipole collectivity seen in other reactions, see Lenske et al. (2019) and Austin et al. (2001). The $L = 3$ multipoles entering in the 2^-, 3^-, 4^-, and 5^- transitions are comparable, while the $L = 5$ components, contributing to the excitations of the 4^- and 5^- states, are the smallest. Thus, an interesting selectivity of the smallest L transfer for this SCE reaction is found. Similar behavior is observed in (^{3}He,t) (Ajzenberg-Selove et al., 1985) and (^{12}C,^{12}N) reactions (von Oertzen, 1988) on the same target, where again the 2^- state is the most populated, thus suggesting a universal property of the nuclear response to the nucleon–nucleon isovector interaction.

The plots in **Figure 4** tell us that the direct SCE mechanism allows the reproduction of the shape of the measured angular distribution. Regarding the absolute cross sections, the data are slightly underestimated in the regions of low excitation, while a good agreement is found in the excitation energy region between 1.7 and 2.6 MeV.

Simple semiclassical estimates for the energy and angular momentum matching for the transfer processes (Brink, 1972) suggest that a cross section of a relevant magnitude may be expected in the region of the ground state, progressively decreasing at higher excitation energies. Thus, the multi-nucleon transfer mechanism is expected to play a major role in the low excitation energy region of the spectrum explaining the larger experimental cross section with respect to the direct mechanism calculations.

CONCLUSIONS

The ^{40}Ca(^{18}O,^{18}F)^{40}K charge exchange reaction, together with the elastic scattering and inelastic scattering of ^{18}O on ^{40}Ca, has been studied at an incident energy of 275 MeV and at forward angles using the MAGNEX spectrometer. The availability of this complete set of data, where the absolute cross section at different angles has been measured with high precision, has allowed a constrained and reliable description of the direct reaction mechanism for the charge exchange process. Charge exchange cross section calculations have been performed in DWBA using a CCEP tested against the elastic and inelastic scattering data and form factors extracted from double folding of a nucleon–nucleon isovector interaction with QRPA transition densities. Such full quantum-mechanical calculations with microscopic nuclear structure inputs describe the order of magnitude and shape of the observed cross sections. Selectivity of this reaction to the different angular momentum transfer components is revealed, making this probe an interesting tool to explore the nuclear response to isovector operators with high momentum as those entering the $0\nu\beta\beta$ NME.

It is worthwhile to emphasize that the above-mentioned calculations are based on a quite involved approach, starting from microscopic nuclear response functions, combined with free-space nucleon–nucleon interactions to derive the transition form factors and fixing ion–ion ISI and FSI by elastic scattering and inelastic scattering. The advantage of such a demanding program is evident from the fact that the data are quite well-described without the need to introduce additional scaling factors, as it was found necessary in the former heavy-ion-induced SCE reactions on the same target such as the ^{40}Ca(^{7}Li,^{7}Be)^{40}K reaction at 35 MeV (Williams-Norton et al., 1979) or the pioneering studies on (^{18}O,^{18}F) on different targets (Kim et al., 1979; Horen et al., 1986; Fifield et al., 1993).

The origin of the remaining difference between the theoretical and experimental results is not easy to access. On a nuclear structure side, there is some room left for refinements of the nuclear response functions by going deeper into the dynamics of polarization effects, e.g., in the multi-phonon approach of Lenske and Tsoneva (2019) or by second RPA methods of Gambacurta et al. (2020). On the reaction side, the competing sequential nucleon transfer mechanism should be studied, mainly for reasons of completeness. Based on the presently available results, a rather successful description of the higher excitation energy region by the direct SCE mechanism strongly hints at a rather insignificant role of nucleon transfer, at least in that spectral region, as indeed it is expected from the matching conditions for transfer processes (Brink, 1972). Nevertheless, the contribution of the transfer mechanism to the SCE process would not prevent any extrapolation to DCE reactions, where transfer processes

are expected to be safely negligible as experimentally checked (Cappuzzello et al., 2015a; Ferreira et al., in preparation) and because they are processes of a higher order than a direct DCE.

DATA AVAILABILITY STATEMENT

The raw data supporting the conclusions of this article will be made available by the authors, without undue reservation.

AUTHOR CONTRIBUTIONS

MCa, JB, SC, CA, SB, FC, DCar, and MCo contributed to conception and design of the study. MCa, SC, CA, FC, DCar, AS, LA, PA-V, TB-L, GB, DCal, VC, EC, IC, FD, HD, CE, PF, SF, MF, AF, MG, AH, FI, RL, NM, MM, JO, AP, LP, HP, FP, GR, OS, SS, VS, GS, DT, ST, AY, and VZ participated to the data taking. SC, ND, and DCar performed the data reduction. JB, SC, HL, JL, and AS performed the calculations. MCa wrote the first draft of the manuscript. JB wrote a section of the manuscript. All authors contributed to manuscript revision, read, and approved the submitted version.

FUNDING

This project has received funding from the European Research Council (ERC) under the European Union's Horizon 2020 Research and Innovation Program (Grant Agreement No. 714625). Partial funding by the European Union's Horizon 2020 research and innovation program under Grant No. 654002 is acknowledged. The grants DGAPA-UNAM IN107820, AG101120, and CONACyT 314857, Mexico, FAPESP (Fundação de Amparo à Pesquisa do Estado de São Paulo, proc. 2019/07767-1), and INCT: Instituto Nacional de Ciência e Tecnologia-Física Nuclear e Aplicações (INCT-FNA, research project 464898/2014-5), Brazil are also acknowledged. HL acknowledges support by INFN and DFG, Grant Le439/16.

REFERENCES

Ajzenberg-Selove, F., Brown, R. E., Flynn, E. R., and Sunier, J. W. (1985). (t,3He) reactions on 40,42,44Ca, 46,48,50Ti, 54Cr, and 54Fe. *Phys. Rev. C* 32, 756–780. doi: 10.1103/PhysRevC.32.756

Akimune, H., Ejiri, H., Hattori, F., Agodi, C., Alanssari, M., Cappuzzello, F., et al. (2020). Spin-dipole nuclear matrix element for the double beta decay of 76Ge by the (He3,t) charge-exchange reaction. *J. Phys. G: Nucl. Part. Phys.* 47:05LT01. doi: 10.1088/1361-6471/ab7a87

Alford, W. P., and Spicer, B. M. (1998). Nucleon charge-exchange reactions at intermediate energy. *Adv. Nucl. Phys.* 1:24. doi: 10.1007/0-306-47073-X_1

Alvarez, M. A. G., Chamon, L. C., Hussein, M. S., Pereira, D., Gasques, L. R., Rossi, J.r., et al. (2003). A parameter-free optical potential for the heavy-ion elastic scattering process. *Nucl. Phys. A* 723, 93–103. doi: 10.1016/S0375-9474(03)01158-8

Anantaraman, N.,Toki, H., and Bertsch, G. F. (1983). An effective interaction for inelastic scattering derived from the Paris potential. *Nucl. Phys. A* 398, 269–278. doi: 10.1016/0375-9474(83)90487-6

Austin, S. M., Adamides, E., Galonsky, A., Nees, T., Sterrenburg, W. A., Bainum, D. E., et al. (2001). Splitting of the dipole and spin-dipole resonances. *Phys. Rev. C* 63:034322. doi: 10.1103/PhysRevC.63.034322

Bellone, J. I., Burrello, S., Colonna, M., Lay, J.-A., and Lenske, H. (2020). Two-step description of heavy ion double charge exchange reactions. *Phys. Lett. B*, 807:135528. doi: 10.1016/j.physletb.2020.135528

Brink, D. M. (1972). Kinematical effects in heavy-ion reactions. *Phys. Lett. B* 40, 37–40. doi: 10.1016/0370-2693(72)90274-2

Calabrese, S., Cappuzzello, F., Carbone, D., and Cavallaro, M. (2020). Analysis of the background on cross section measurements with the MAGNEX spectrometer:The (20Ne,20O) Double Charge Exchange case. *Nucl. Inst. Meth. Phys. Res. A* 980:164500. doi: 10.1016/j.nima.2020.164500

Cappuzzello, F., Agodi, C., Bondì, M., Carbone, D., Cavallaro, M., Cunsolo, A., et al. (2014). A broad angular-range measurement of elastic and inelastic scatterings in the 16O on 27Al reaction at 17.5 MeV/u. *Nucl. Instr. Meth. A* 763, 314–319. doi: 10.1016/j.nima.2014.06.058

Cappuzzello, F., Agodi, C., Carbone, D., and Cavallaro, M. (2016). The MAGNEX spectrometer: Results and perspectives. *Eur. Phys. J. A* 52:169. doi: 10.1140/epja/i2016-16167-1

Cappuzzello, F., Agodi, C., Cavallaro, M., Carbone, D., Tudisco, S., Lo Presti, D., et al. (2018). The NUMEN project: NUclear Matrix Elements for neutrinoless double beta decay. *Eur. Phys. J. A* 54:72. doi: 10.1140/epja/i2018-12509-3

Cappuzzello, F., Carbone, D., and Cavallaro, M. (2011). Measuring the ions momentum vector with a large acceptance magnetic spectrometer. *Nucl. Instrum. Methods A* 638, 74–82. doi: 10.1016/j.nima.2011.02.045

Cappuzzello, F., Carbone, D., Cavallaro, M., Bond,ì, M., Agodi, C., Azaiez, F., et al. (2015b). Signatures of the giant pairing vibration in the 14C and 15C atomic nuclei. *Nat. Commun.* 6:6743. doi: 10.1038/ncomms7743

Cappuzzello, F., and Cavallaro, M. (2020). Nuclear response to second-order isospin probes in connection to double beta decay. *Universe* 6:217. doi: 10.3390/universe6110217

Cappuzzello, F., Cavallaro, M., Agodi, C., Bond,ì, M., Carbone, D., et al. (2015a). Heavy-ion double charge exchange reactions: a tool toward 0nbb nuclear matrix elements. *Eur. Phys. J. A* 51:145. doi: 10.1140/epja/i2015-15145-5

Cappuzzello, F., Cavallaro, M., Cunsolo, A., Foti, A., Carbone, D., et al. (2010). A particle identification technique for large acceptance spectrometers. *Nucl. Instrum. Methods A* 621, 419–423. doi: 10.1016/j.nima.2010.05.027

Cappuzzello, F., Lenske, H., Cunsolo, A., Beaumel, D., Fortier, S., Foti, A., et al. (2004a). Analysis of the 11B(7Li, 7Be)11Be reaction at 57 MeV in a microscopic approach. *Nuclear Phys. A* 739, 30–56. doi: 10.1016/j.nuclphysa.2004.03.221

Cappuzzello, F., Orrigo, S. E. A., Cunsolo, A., Lenske, H., Allia, M. C., Beaumel, D., et al. (2004b). Excited states of 15C. *Europhys. Lett.* 65, 766–772. doi: 10.1209/epl/i2003-10197-8

Carbone, D. (2015). Signals of the Giant Pairing Vibration in 14C and 15C nuclei populated by (18O,16O) two-neutron transfer reactions. *Eur. Phys. J. Plus.* 130 143. doi: 10.1140/epjp/i2015-15143-0

Carbone, D., Ferreira, J. L., Calabrese, S., Cappuzzello, F., Cavallaro, M., Hacisalihoglu, A., et al. (2020). Analysis of two-nucleon transfer reactions in the 20Ne+116Cd system at 306 MeV. *Phys. Rev. C* 102:044606. doi: 10.1103/PhysRevC.102.044606

Carbone, D., Ferreira, J. L., Cappuzzello, F., Lubian, J., Agodi, C., et al. (2017). Microscopic cluster model for the description of new experimental results on the 13C(18O,16O)15C two-neutron transfer at 84 MeV incident energy. *Phys. Rev. C* 95:034603. doi: 10.1103/PhysRevC.95.034603

Carbone, D., Linares, R., Amador-Valenzuela, P., Calabrese, S., Cappuzzello, F., Cavallaro, M., et al. (2021). Initial state interaction for the 20Ne+130Te and 18O+116Sn Systems at 15.3 AMeV from elastic and inelastic scattering. *Measur. Univ.* 7:58. doi: 10.3390/universe7030058

Cardozo, E. N., Lubian, J., Linares, R., Cappuzzello, F., Carbone, D., Cavallaro, M., et al. (2018). Competition between direct and sequential two-neutron transfers in the 18O + 28Si collision at 84 MeV. *Phys. Rev. C* 97:064611. doi: 10.1103/PhysRevC.97.064611

Cavallaro, M. (2011). Preliminary study of the 19F(7Li, 7Be)19O reaction at 52MeV with MAGNEX. *Nuovo Cimento* 34, 1–9. doi: 10.1393/ncc/i2011-10924-8

Cavallaro, M., Aciksoz, E., Acosta, L., Agodi, C., Auerbach, N., Bellone, J., et al. (2017). NURE: an ERC project to study nuclear reactions for neutrinoless double beta decay. *Proc. Sci.* 302:015. doi: 10.22323/1.302.0015

Cavallaro, M., Cappuzzello, F., Bond,ì, M., Carbone, D., Garcia, V. N., Gargano, A., et al. (2013). Quantitative analysis of two-neutron correlations in the 12C(18O,16O)14C reaction. *Phys. Rev. C* 88:054601. doi: 10.1103/PhysRevC.88.054601

Cavallaro, M., Cappuzzello, F., Carbone, D., Cunsolo, A., Foti, A., Khouaja, A., et al. (2012). The low-pressure focal plane detector of the MAGNEX spectrometer. *Eur. Phys. J. A* 48:59. doi: 10.1140/epja/i2012-12059-8

Cavallaro, M., Cappuzzello, F., Carbone, D., Cunsolo, A., Foti, A., Linares, R., et al. (2011). Transport efficiency in large acceptance spectrometers. *Nucl. Instr. Meth. A* 637, 77–87. doi: 10.1016/j.nima.2011.01.078

Chamon, L. C., Carlson, B. V., Gasques, L. R., Pereira, D., De Conti, C., Alvarez, M. A. G., et al. (2002). Toward a global description of the nucleus-nucleus interaction. *Phys. Rev. C* 66:014610. doi: 10.1103/PhysRevC.66.014610

Crema, E., Otomar, D. R., Simões, R. F., Barioni, A., Monteiro, D. S., Ono, L. K., et al. (2011). Near-barrier quasielastic scattering as a sensitive tool to derive nuclear matter diffuseness. *Phys. Rev. C* 84:024601. doi: 10.1103/PhysRevC.84.024601

Diel, F., Fujita, Y., Fujita, H., Cappuzzello, F., Ganioglu, E., Greweet, E.-W., et al. (2019). High-resolution study of the Gamow-Teller strength in the 64Zn(3He,t)64Ga reaction. *Phys. Rev. C* 99:054322. doi: 10.1103/PhysRevC.99.054322

Douma, C. A., Agodi, C., Akimune, H., Alanssari, M., Cappuzzello, F., Carbone, D., et al. (2020). Gamow–Teller strength distributions of 116Sb and 122Sb using the (3He, t) charge-exchange reaction. *Eur. Phys. J. A* 56:51. doi: 10.1140/epja/s10050-020-00044-9

Ejiri, H. (2005). Double beta decays and neutrino masses. *Phys. Soc. Jpn.* 74, 2101–2127. doi: 10.1143/JPSJ.74.2101

Ejiri, H., Soukouti, N., and Suhonen, J. (2014). Spin-dipole nuclear matrix elements for double beta decays and astro-neutrinos. *Phys. Lett. B* 729, 27–32. doi: 10.1016/j.physletb.2013.12.051

Ejiri, H., Suhonen, J., and Zuber, K. (2019). Neutrino–nuclear responses for astro-neutrinos, single beta decays and double beta decays. *Phys. Rep.* 1:797. doi: 10.1016/j.physrep.2018.12.001

Ermamatov, M. J., Cappuzzello, F., Lubian, J., Cubero, M., Agodi, C., Carbone, D., et al. (2016). Two-neutron transfer analysis of the 16O(18O,16O)18O reaction. *Phys. Rev. C* 94:024610. doi: 10.1103/PhysRevC.94.024610

Ermamatov, M. J., Linares, R., Lubian, J., Ferreira, L., Cappuzzello, F., Carbone, D., et al. (2017). Comprehensive analysis of high-lying states in 18O populated with (t, p) and (18O,16O) reactions. *Phys. Rev. C* 96:044603. doi: 10.1103/PhysRevC.96.044603

Ferreira, J. L., Carbone, D., Cavallaro, M., Deshmukh, N. N., Agodi, C., and Brischetto, G. A. (2021). Analysis of two-proton transfer in the 40Ca(18O,20Ne)38Ar reaction at 270 MeV. *Phys. Rev. C.*

Fifield, L. K., Catford, W. N., Orr, N. A., Ophel, T. R., Etchegoyen, A., and Etchegoyen, M. C. (1993). Charge-exchange reactions on 36S. *Nucl. Phys. A* 552, 125–139. doi: 10.1016/0375-9474(93)90335-U

Fonseca, L. M., Linares, R., Zagatto, V. A. B., Cappuzzello, F., Carbone, D., Cavallaro, M., et al. (2019). Elastic and inelastic scattering of 16O on 27Al and 28Si at 240 MeV. *Phys. Rev. C* 100:014604. doi: 10.1103/PhysRevC.100.014604

Franey, M. A., and Love, W. G. (1985). Nucleon-nucleon t-matrix interaction for scattering at intermediate energies. *Phys. Rev. C* 31:488. doi: 10.1103/PhysRevC.31.488

Frekers, D., Puppe, P., Thies, J. H., and Ejiri, H. (2013). Gamow–Teller strength extraction from (3He, t) reactions. *Nuclear Phys A* 916, 219–240. doi: 10.1016/j.nuclphysa.2013.08.006

Fujita, H., Fujita, Y., Adachi, T., Bacher, A. D., Berg, G. P. A., et al. (2007). Isospin structure of Jπ =1+states in 58Ni and 58Cu studied by 58Ni(p,p') and 58Ni(3He,t)58Cu measurements. *Phys. Rev. C* 75:034310. doi: 10.1103/PhysRevC.75.034310

Fujita, Y., Hatanaka, K., Berg, G. P. A., Hosono, K., Matsuo, N., Morinobu, S., et al. (1997). Matching of a beam line and a spectrometer New beam line project at RCNP. *Nucl. Instrum. Methods Phys. Res. B* 126, 274–278. doi: 10.1016/S0168-583X(96)01008-7

Fujita, Y., Rubio, B., and Gelletly, W. (2011). Spin–isospin excitations probed by strong, weak and electro-magnetic interactions. *Progr. Particle Nuclear Phys.* 66, 549–606. doi: 10.1016/j.ppnp.2011.01.056

Gambacurta, D., Grasso, M., and Engel, J. (2020). Gamow-teller strength in 48Ca and 78Ni with the charge-exchange subtracted second random-phase approximation. *Phys. Rev. Lett.* 125:212501. doi: 10.1103/PhysRevLett.125.212501

Horen, D. J., Burks, B. L., Fernandes, M. A. G., Auble, R. L., Bertrand, F. E., Blankenship, J. L., et al. (1986). Investigation of the one-step direct contribution to the 28Si (18O, 18F) 28Al reaction at 19.6 MeV/nucleon. *Phys. Lett. B* 181, 38–42. doi: 10.1016/0370-2693(86)91250-5

Jokiniemi, L., Suhonen, J., Ejiri, H., and Hashim, I. H. (2019). Pinning down the strength function for ordinary muon capture on 100Mo. *Phys. Lett. B*, 794, 143–147. doi: 10.1016/j.physletb.2019.05.037

Khoa, D. T., and Satchler, G. R. (2000). Generalized folding model for elastic and inelastic nucleus–nucleus scattering using realistic density dependent nucleon–nucleon interaction. *Nucl. Phys. A* 668, 3–41. doi: 10.1016/S0375-9474(99)00680-6

Kibedi, T., and Spear, R. H. (2002). Atomic data and nuclear data *Tables* 80, 35–82. doi: 10.1006/adnd.2001.0871

Kim, B. T., Greiner, A., Fernandes, M. A. G., Lisbona, N., Low, K. S., and Mermaz, M. C. (1979). Heavy-ion charge exchange reaction 28Si(18O,18F)28Al. *Phys. Rev. C* 20:1396–1407. doi: 10.1103/PhysRevC.20.1396

Lenske, H. (1988). Theory of heavy ion charge exchange scattering at low and intermediate energies. *Nucl. Phys. A* 482, 343c–356c. doi: 10.1016/0375-9474(88)90595-7

Lenske, H., Bellone, J. I., Colonna, M., and Lay, J.-A. (2018). Theory of single-charge exchange heavy-ion reactions. *Phys. Rev. C* 98:044620. doi: 10.1103/PhysRevC.98.044620

Lenske, H., Cappuzzello, F., Cavallaro, M., and Colonna, M. (2019). Heavy ion charge exchange reactions as probes for nuclear beta-decay. *Progress Part. Nuclear Phys.* 109:103716. doi: 10.1016/j.ppnp.2019.103716

Lenske, H., and Tsoneva, N. (2019). Dissolution of shell structures and the polarizability of dripline nuclei. *Eur. Phys. J. A* 55:238. doi: 10.1140/epja/i2019-12811-6

Linares, R., Ermamatov, M. J., Lubian, J., Cappuzzello, F., Carbone, D., Cardozo, E. N., et al. (2018). Analysis of the one-neutron transfer to 16O, 28Si, and 64Ni induced by the (18O,17O) reaction at 84 MeV. *Phys. Rev C.* 98:054615. doi: 10.1103/PhysRevC.98.054615

Lubian, J., and Nunes, F. M. (2007). Searching for a polarization potential in the breakup of ^{8}B. *J. Phys. G: Nucl. Part. Phys.* 34, 513–521. doi: 10.1088/0954-3899/34/3/009

Nociforo, C., Cappuzzello, F., Cunsolo, A., Foti, A., Orrigo, S. E. A., Winfield, J. S., et al. (2006). Exploring the Nα+3n light nuclei via the (7Li,7Be) reaction. *Eur. Phys. J. A* 27, 283–288. doi: 10.1007/3-540-32843-2_43

Ohkubo, S., and Hirabayashi, Y. (2014). Evidence for a secondary bow in Newton's zero-order nuclear rainbow. *Phys. Rev. C* 89:051601(R). doi: 10.1103/PhysRevC.89.051601

Oliveira, J. R. B., Cappuzzello, F., Chamon, L. C., Pereira, D., Agodi, C., Bond,í M., et al. (2013). Study of the rainbow-like pattern in the elastic scattering of 16O on 27Al at Elab.= 100 MeV. *J. Phys. G: Nucl. Part. Phys.* 40:105101. doi: 10.1088/0954-3899/40/10/105101

Osterfeld, F. (1992). Nuclear spin and isospin excitation. *Rev. Modern Phys.* 64, 491–557. doi: 10.1103/RevModPhys.64.491

Paes, B., Santagati, G., Magana Vsevolodovna, R., Cappuzzello, F., Carbone, D., Cardozo, E. N., et al. (2017). Long-range versus short-range correlations in the two-neutron transfer reaction 64Ni(18O,16O)66Ni. *Phys. Rev. C* 96:044612. doi: 10.1103/PhysRevC.96.044612

Pereira, D., Lubian, J., Oliveira, J. R. B., de Sousa, D. P., Chamon, L. C., et al. (2009). An imaginary potential with universal normalization for dissipative processes in heavy-ion reactions. *Phys. Lett. B* 670, 330–335. doi: 10.1016/j.physletb.2008.10.066

Pritychenko, B., Birch, M., Singh, B., and Horoi, M. (2016). Tables of E2 transition probabilities from the first 2+ states in even–even nuclei. *At. Data Nucl. Data Tables* 107:1. doi: 10.1016/j.adt.2015.10.001

Pritychenko, B., Birch, M., Singh, B., and Horoi, M. (2017). Erratum to Tables of E2 transition probabilities from the first 2+ states in even-even nuclei. *At. Data Nucl. Data Tables* 114:371. doi: 10.1016/j.adt.2016.08.002

Rangel, J., Lubian, J., Canto, L. F., and Gomes, P. R. S. (2016). Effect of Coulomb breakup on the elastic cross section of the 8B proton-halo projectile on a heavy, 208Pb target. *Phys. Rev. C* 93:054610. doi: 10.1103/PhysRevC.93.054610

Santopinto, E., García-Tecocoatzi, H., Magaña Vsevolodovna, R. I., and Ferretti, J. (2018). Heavy-ion double-charge-exchange and its relation to neutrinoless double-beta decay. *Phys. Rev. C* 98:061601. doi: 10.1103/PhysRevC.98.061601

Satchler, G. R. (1983). *Direct Nuclear Reactions.* Oxford: Oxford University Press.

Spatafora, A., Cappuzzello, F., Carbone, D., Cavallaro, M., Lay, J. A., Acosta, L., et al. (2019). 20Ne+76Ge elastic and inelastic scattering at 306 MeV. *Phys. Rev. C* 100:034620. doi: 10.1103/PhysRevC.100.034620

Taddeucci, T. N., Goulding, C. A., Carey, T. A., Byrd, R. C., Goodman, D. C., Gaarde, C., et al. (1987). The (p, n) reaction as a probe of beta decay strength. *Nucl. Phys. A* 469, 125–172. doi: 10.1016/0375-9474(87)90089-3

Thompson, I. J. (1988). Getting started with FRESCO. *Comput. Phys. Rep.* 7, 167–211. doi: 10.1016/0167-7977(88)90005-6

Thompson, I. J., Nagarajan, M. A., Lilley, J. S., and Fulton, B. R. (1985). Contribution of multistep transfers to low-energy elastic and reaction cross sections. *Phys. Lett. B* 157:250. doi: 10.1016/0370-2693(85)90660-4

Thompson, I. J., Nagarajan, M. A., Lilley, J. S., Smithson, M. J., et al. (1989). The threshold anomaly in 16O+208Pb scattering. *Nucl. Phys. A* 505,84–102. doi: 10.1016/0375-9474(89)90417-X

Torresi, D., Sgouros, O., Soukeras, V., Cavallaro, M., Cappuzzello, F., Carbone, D., et al. (2021). An upgraded focal plane detector for the MAGNEX spectrometer. *Nucl. Instr. and Meth. A* 989:164918. doi: 10.1016/j.nima.2020.164918

von Oertzen, W. (1988). Excitation of isovector modes in heavy ion induced charge exchange reactions. *Nucl. Phys. A* 482, 357c–372c. doi: 10.1016/0375-9474(88)90596-9

Williams-Norton, M. E., Petrovich, F., Kemper, K. W., Puigh, R. J., Stanley, D., et al. (1979). Charge exchange study with the 40Ca(7Li, 7Be)40K reaction. *Nucl. Phys. A* 313, 477–484. doi: 10.1016/0375-9474(79)90514-1

Zagatto, V. A. B., Cappuzzello, F., Lubian, J., Cavallaro, M., Linares, R., Carbone, D., et al. (2018). Important role of projectile excitation in 16O + 60Ni and 16O + 27Al scattering at intermediate energies. *Phys. Rev. C* 97:054608. doi: 10.1103/PhysRevC.97.054608

Conflict of Interest: The authors declare that the research was conducted in the absence of any commercial or financial relationships that could be construed as a potential conflict of interest.